Numeric Simulation of Frequency-dependent Seismic Response and Hydrocarbon Detection, a Turbidite Reservoir in

JZ Area, the Bohai Sea, China

Xuehua Chen[1]; Zhenhua He[1]; Xilei He[1] (1) State Key Laboratory of Oil & Gas Reservoir Geology and Exploitation, Chengdu University of Technology, Chengdu 610059, China; Deji Hunag[2] (2) College of Geophysics, Chengdu University of Technology, Chengdu 610059, China

ABSTRACT

The numerous recent laboratory and field examples show the potential benefits of seismic low frequencies in hydrocarbon detection. To simulate the frequency-dependent response of turbidite reservoirs in JZ Area, the Bohai Sea, China, and then implement frequency-dependent detection of the hydrocarbon accumulation based on low frequencies, we expanded a diffusive and viscous wave equation (DVWE), which takes into account the diffusive and viscous attenuation, and velocity dispersion in fluid-bearing poroelastic media. In design of the reservoir equivalent geologic model, by applying a 90º-phase shift on the raw seismic section contained turbidites, we pick zero crossing on converted section to produce interface (reflectivity) section. We then assign the parameters such as density, velocity, diffusive, viscosity, and Q for each stratum to produce a physical parameters section. Such parameters originate from the well log and rock physical experiments. The DVWE-based simulation result not only shows the characteristic reflection and geometry of turbidites, that are consistent desirably with the reflection feature on the raw seismic section, but also delineates the phase delay, instantaneous dominant frequency decrease and magnitude attenuation related to the gas-bearing reservoir. By conducting instantaneous spectral decomposition on the simulation section, the common frequency sections indicate bright strong energy of the gas reservoir and low-frequency shadow lie immediately underneath the reservoir at 8Hz and 12Hz. At 20Hz and 28Hz, the gas reservoir is brighter than the shadow that becomes weaker but still persists. The shadow is almost gone at 36Hz.

We carry out instantaneous spectral decomposition and calculate fluid mobility (permeability to viscosity ratio) on the seismic data. At 12Hz, the hydrocarbon accumulation in tubidites show clear bright spot on common frequency section and horizon slice at the reservoir. There show abnormally strong low-frequency shadow on the common section and the slice for a 40ms window immediately below the reservoir. At 20-36Hz, the reservoir remains bright, and the shadow has gradually disappeared. The fluid mobility calculated at 12Hz also clearly delineates the bright gas reservoir and its spatial distribution.

In this case study presented above, the low-frequency effects are especially important for delineation of the fluid signature. It is necessary to develop more numerous deeper experiments and theoretical research in the near future.

INTRODUCTION

It has been found for many years that low-frequency seismic signals can be successfully

used for accurate delineation of hydrocarbon reservoirs. This frequency dependence of seismic reflections from fluid-saturated porous media has been detected in different geologic environments. The numerous recent laboratory and field examples show the potential benefits of seismic low frequencies anomalies in hydrocarbon detection. Taner et al.(1979) once noted in complex seismic trace analysis that the lower apparent frequency occur from reflection immediately underneath the petroliferous zone. The low-frequency shadow (LFS) is often observed on common frequency sections decomposed by instantaneous spectral analysis (Castagna et al., 2003; Wang, 2007; Liu and Marfurt, 2007; Chen et al., 2009). However, although Ebrom (2004) summarized ten possible factors responsible for this phenomenon. There are still no definite explanations about its mechanism (Tai et al., 2009). It is necessary for understanding its mechanism to further theoretically study and numerically simulate (Liu, 2004). Goloshubin and Korneev (2000; 2002; 2004) studied the seismic response of fluid-saturated porous media by a series of rock physical model experiments. Their observations in laboratory indicate that reflections from a fluid-saturated layer have increased amplitude and delayed traveltime at low frequencies. They proposed a 1D scalar diffusive and viscous wave-propagation equation, but they did not study its numeric implementation.

Another low-frequencies-dependent hydrocarbon indication is the fluid mobility (permeability to viscosity ratio), which is velocity dispersion dependent due to the hydrocarbon-saturated reservoirs. Silin et al. (2004) derived an asymptotic scaling of the frequency-dependent component of the reflection coefficient with respect to a dimensionless parameter depending on the reservoir fluid mobility. Goloshubin et al. (2008) used fluid mobility to estimate the permeability of reservoirs.

In this paper, we present a 3D diffusive and viscous wave equation (DVWE), and simulate the frequency-dependent seismic response on the geological model, which is created by integrating real seismic data, rock physics and well log. By following the guidance of this simulation, we use both LFS and fluid mobility to indicate the hydrocarbon in a turbidite reservoir from JZ Area, the Bohai Sea, China.

THEORY AND METHODS

Seismic data based geological model building

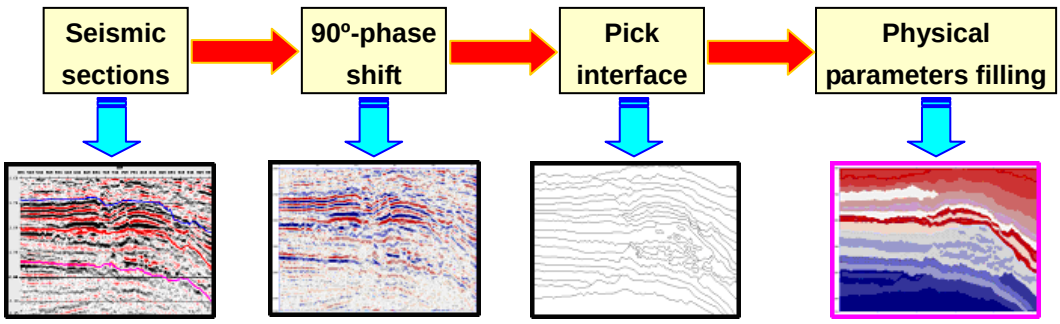

Figure 1 Schematic workflow of the model building

In the equivalent geological model building, we firstly transform the raw seismic sections contained my target interval by applying a 90º-phase shift, which have superior geologic interpretive advantages for thin bed mapping that advocated by Zeng and Backus (2005). Next,

we automatically pick zero crossing on the converted sections to produce interface (reflectivity) sections. We then assign the physical parameters such as the density, velocity, diffusiveness, viscosity, and Q of the fluid and skeleton for each stratum, and produce physical parameters sections. Such parameters originate from the well log and rock physical experiments. The schematic workflow of the seismic data based geological model building is given in Figure 1.

Diffusive and Viscous Wave Equation (DVWE)

Considering the diffusiveness and viscosity of the fluid, Goloshubin and Korneev proposed a 1D scalar diffusive and viscous wave-propagation equation, which is given by (Goloshubin et al., 2000; Goloshubin et al., 2002; Korneev et al., 2004)

$$\frac{\partial^2 u}{\partial t^2} + \zeta \frac{\partial u}{\partial t} - \eta \frac{\partial^3 u}{\partial z^2 \partial t} - v^2 \frac{\partial^2 u}{\partial z^2} = 0 \tag{1}$$

where u is the displacement, ζ is diffusive attenuation parameter in unit of Hz, η is viscous attenuation parameter in unit of m^2/s, and v is the wave-propagation velocity in unit m/s.

We generalize equation (1) and obtain its 3D form, which can be expressed as

$$\begin{aligned} \frac{\partial^2 u}{\partial t^2} + \zeta\,(x,y,z)\frac{\partial u}{\partial t} - \eta\,(x,y,z)\left(\frac{\partial^3 u}{\partial x^2 \partial t} + \frac{\partial^3 u}{\partial y^2 \partial t} + \frac{\partial^3 u}{\partial z^2 \partial t}\right) \\ - v^2\,(x,y,z)\left(\frac{\partial^2 u}{\partial x^2} + \frac{\partial^2 u}{\partial y^2} + \frac{\partial^2 u}{\partial z^2}\right) = 0 \end{aligned} \tag{2}$$

If $\zeta(x,y,z) = 0$ and $\eta(x,y,z) = 0$, equation (2) is equivalent to the conventional acoustic wave equation. We can implement this equation in a numeric simulation by using wavefield extrapolation solution in frequency-wavenumber domain. Note that v is assigned the frequency-dependent velocity because of the usual dispersion related to hydrocarbon saturated reservoirs (Chapman et al., 2005; Odebeatu et al., 2006; Liu, 2004).

Fluid mobility

The fluid mobility measurement can be retrieved from the seismic reflected signal at low frequencies. Silin et al. (2004) obtained an asymptotic representation of the seismic reflection from a fluid-saturated porous medium in the low-frequency domain. It turned out that the frequency-dependent component of the reflection coefficient is proportional to the square root of the product of frequency of the signal and the fluid mobility of the reservoir. This asymptotic expression of the reflection coefficient is given by

$$R = R_0 + R_1(1+i)\sqrt{\frac{\kappa\rho_f}{\eta}\omega} \tag{3}$$

where R_0 and R_1 are real coefficients, which are the dimensionless functions of the mechanical properties such as the porosity, the density, and the elastic modulus of both the fluid and rock. κ denotes the permeability of the reservoir; η is the fluid viscosity; ρ_f denotes the density of the fluid in reservoirs; ω is the angular frequency of the seismic wave, and $i = \sqrt{-1}$.

Suppose we are given the fluid mobility of reservoirs $\mathbb{F} = \frac{\kappa}{\eta}$, we can calculate it by using

the equation in the following form

$$\mathbb{F} \approx \frac{1}{\mathbb{C}^2}\left[\frac{\partial a(\omega)}{\partial \omega}\right]^2 \omega \tag{4}$$

where the coefficient $\mathbb{C}$ is a complex function of the mechanical properties of both the fluid and the skeleton. $a(\omega)$ is instantaneous spectral amplitude at an optimal low angular frequency ω at which the reflection coefficient in equation (3) attains its maximum.

FIELD DATA EXAMPLE

The methodology and workflow described in this paper is now applied to delineate the turbidite hydrocarbon reservoir from JZ Area, the Bohai Sea, China. The raw seismic section and the slice in the target interval are shown in Figure 2. We first build the geological model from the raw seismic section in Figure 2a by using my workflow of the model building. The DVWE-based simulation section of this model is shown in Figure 3a, in which the seismic response features in the target interval show high correlation with the raw section in Figure 2a. We do the instantaneous spectral decomposition on the simulation section based on the generalized S transform (Chen et al., 2009).The common frequency section indicates bright strong energy of the gas reservoir (indicated by a green arrow) and the LFS (indicated by a black contours) lie immediately underneath the reservoir at 8Hz (Figure 3b). At 12Hz and 20Hz, the shadow becomes weak (Figure 3c-d), and the LFS has gradually disappeared at 28Hz and 36Hz (Figure 3e-f). However, note that the gas reservoir is still bright on these sections, and the spectral magnitude underneath the bottom of the horizon “Low” has gradually attenuated due to the energy loss of the seismic waveform in propagating the turbidite.

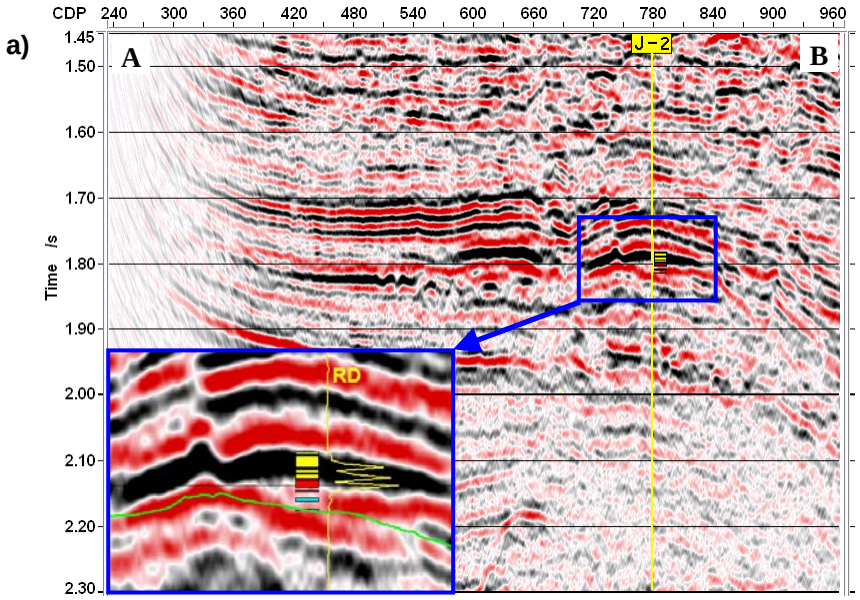

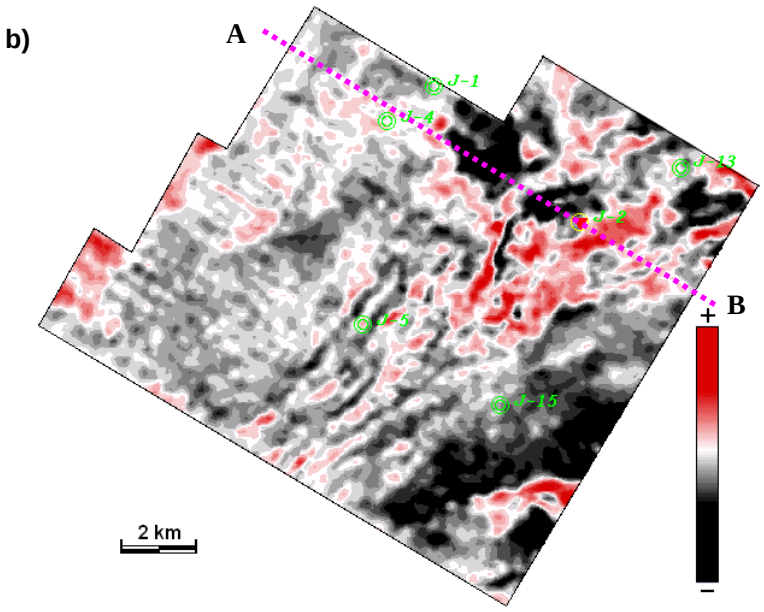

Figure 2 (a) Stacked seismic section and the RD log of well J-2, where , and denote gas, oil and brine, respectively; (b) seismic slice extracted through the turbidite gas reservoir in the target interval. (Original seismic data courtesy of CNOOC)

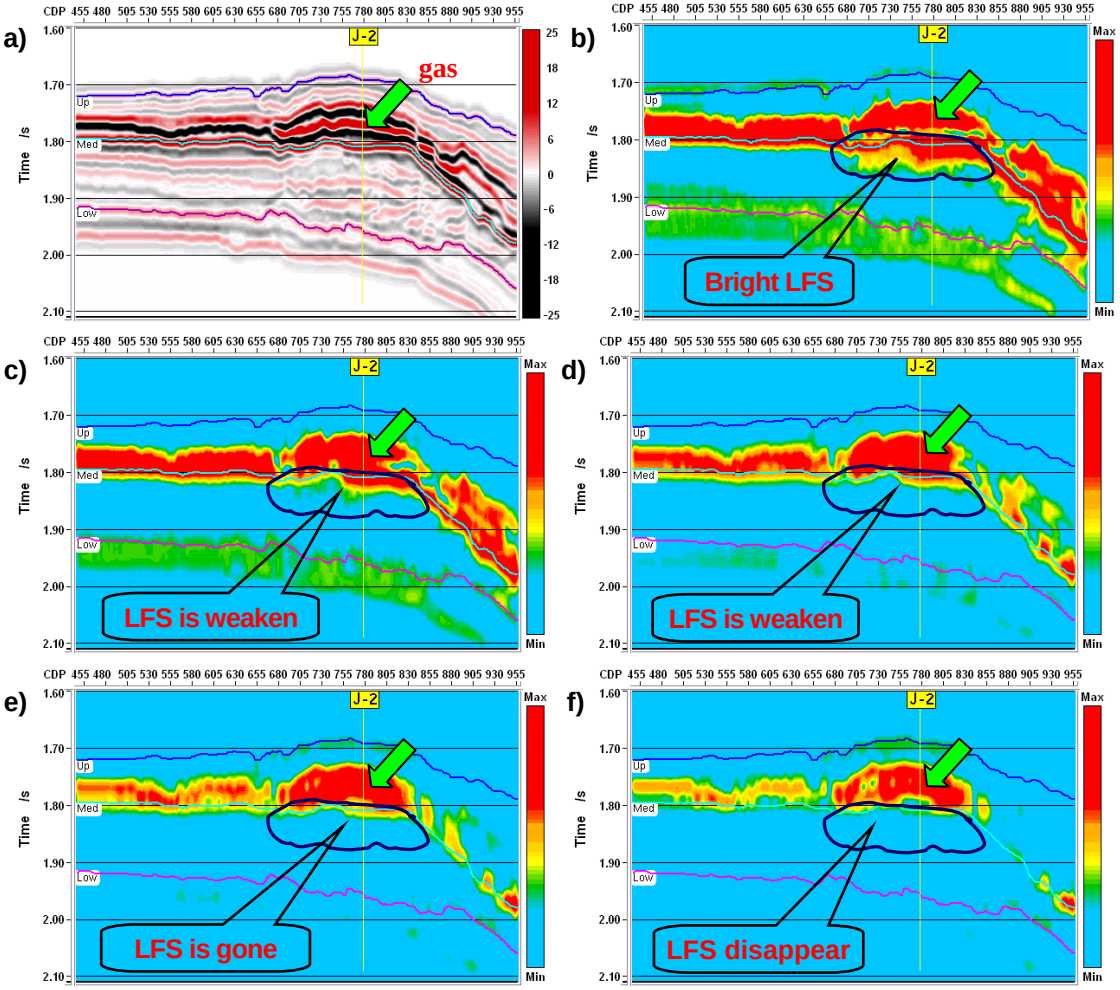

Figure 3 (a) Numerical simulation seismic section corresponding to the geological model

based on the stacked seismic section in Figure 2, and the instantaneous spectral sections at (b) 8Hz, (c) 12Hz, (d) 20Hz, (e) 28Hz and (f) 36Hz. Figure 3b shows strong LFS (outlined by a black contour) lie immediately underneath the reservoir (indicated by a green arrow). The LFS has gradually attenuated at 12Hz and 20Hz. The LFS has disappeared whereas the reservoir is still bright at 28Hz and 36Hz.

The instantaneous spectral sections and slices decomposed from the real stacked seismic data are both shown in Figure 4 and Figure 5. At 12Hz, the hydrocarbon accumulation in the tubidite show clear bright spot (indicated by a green arrow), and significant LFS (indicated by a black contour) occurs beneath the reservoir on the spectral section in Figure 4a. The LFS is gradually attenuated at 20Hz and 28Hz (Figure 4b and Figure 4c), and it is almost gone at 36Hz (Figure 4d) while the bright reservoirs still persist. Note that Figure 4 is consistent desirably with Figure 3 in the frequency-dependent instantaneous spectral features.

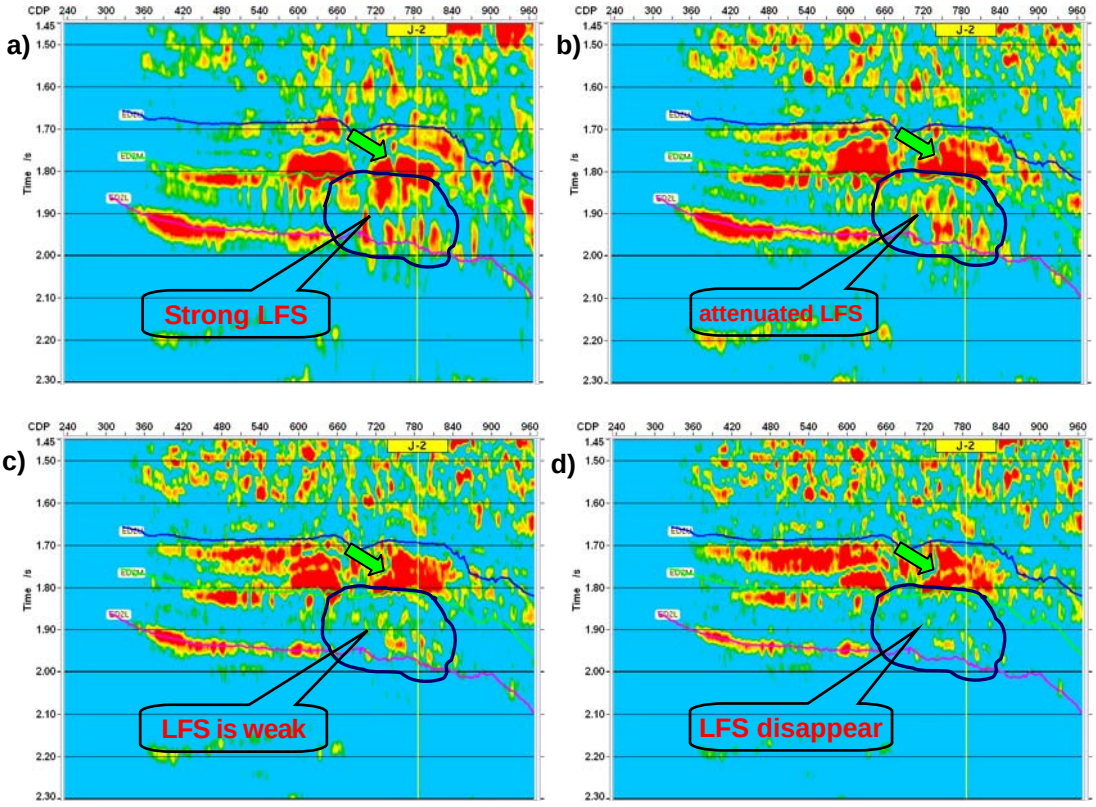

Figure 4 The instantaneous spectral sections corresponding to the stacked seismic section in Figure 2. (a) 12Hz section, it shows the bright gas reservoir (indicated by a green arrow) and strong LFS (outlined by a black contour) lie immediately underneath the reservoir; (b) 20Hz, note that the LFS become weak; (c) 28Hz, and (d) 36Hz, shown that the gas reservoir is still bright whereas LFS has disappeared.

The 12Hz spectral slices in Figure 5a indicate the reservoir dimensions and the extent of the strong LFS below the reservoir (both outlined by black contours). The abnormally strong LFS is attenuated at 20Hz (Figure 5b). It has gradually disappeared at 28Hz and 36Hz (Figure 5c-d). At the same time, the reservoirs are still bright spots on the left column of the slices in

Figure 5.

The fluid mobility calculated at 12Hz also clearly delineates the bright gas reservoir (indicated by a green arrow) and its spatial distribution (outlined by dashed contours) in Figure 6. The hydrocarbon anomalies indicated by the fluid mobility measurement are almost identical with the LFS delineation in both Figure 4 and Figure 5.

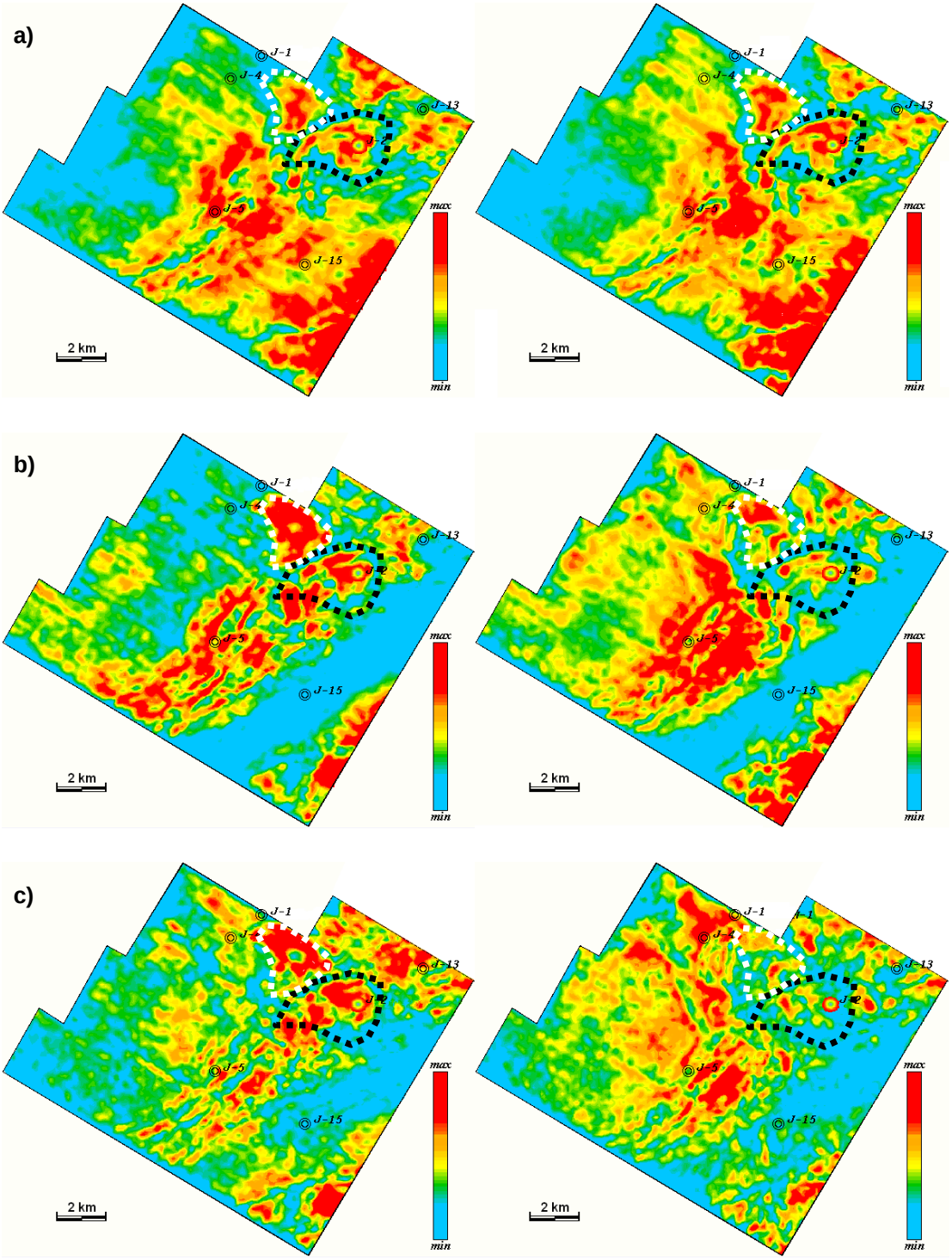

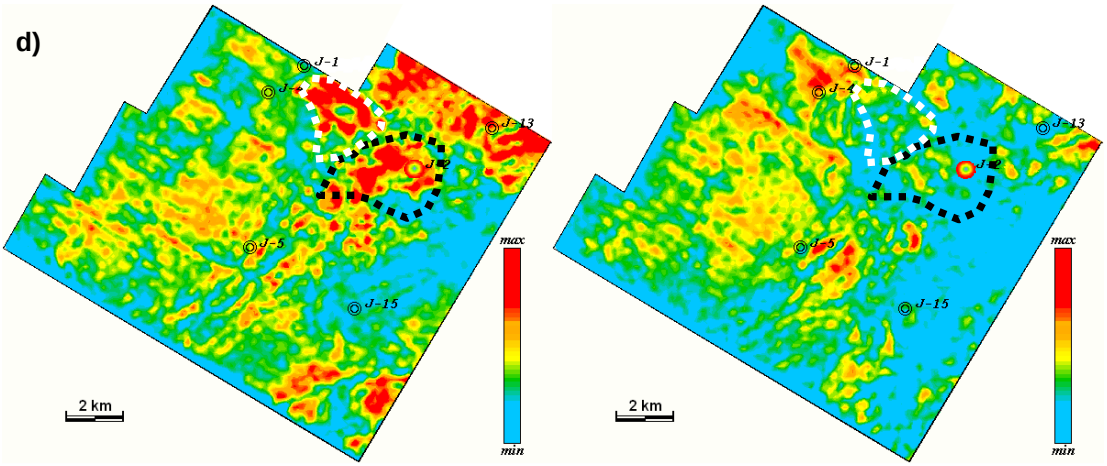

Figure 5 The instantaneous spectral slices (left column) through the turbidite reservoir in the target interval and for a 40-ms window immediately below the reservoir base (right column). Note that the dashed contours outline the range of reservoirs. (a) At 12Hz, two strong events are apparent on the slices, one determines the reservoir dimensions (left) and another indicates the shadow (right). (b) 20Hz slice. The reservoir is still bright (left) whereas the shadow becomes weak (right). (c) and (d) are 28Hz and 36Hz slices, respectively. The reservoir remains bright (left), and the LFS has been gone (right).

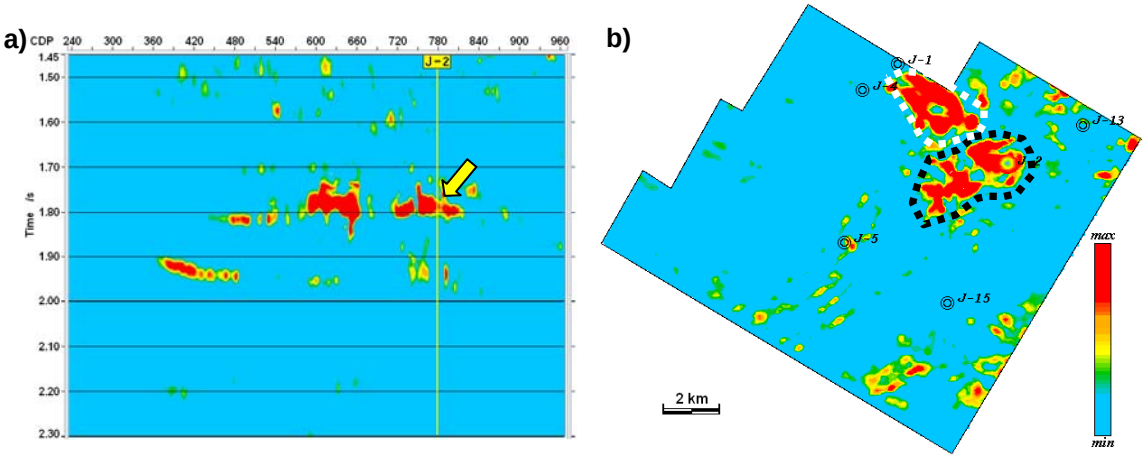

Figure 6 (a) The fluid mobility section corresponding to the stacked seismic section in Figure 2, and (b) the fluid mobility slice extracted through the turbidite gas reservoir. Note that the significant anomalies (indicated by the yellow arrow and dashed contours) are shown on the maps.

CONCLUSION

The DVWE-based simulation workflow presented in this paper not only shows the characteristic reflection and geometry of the turbidite, it also delineates the frequency-dependent features such as the LFS and the instantaneous spectral energy attenuation of the seismic reflection related to the hydrocarbon reservoirs. This workflow can be used as guidance in frequency-dependent fluid indication.

In our case study presented above, the low-frequency effects are especially important for delineating the fluid signature. It is necessary to develop the numerous deeper experiments

and theoretical research in the near future.

ACKNOWLEDGEMENTS

This work was supported by the National Natural Science Foundation of China under grant No. 41004054, the Research Fund for the Doctoral Program of Higher Education of China (grant No. 20105122120002) and the Cultivating Program of Middle-aged Backbone Teachers of Chengdu University of Technology. The authors would like to express their sincere thanks to the China National Offshore Oil Corp. (CNOOC) for supplying the marine seismic data. The authors also acknowledge their colleague Dr. Cai Hanpeng, Dr. Zhao Yan and Dr. Bai Min for their useful discussion and assistances in this research.

REFERENCES

Castagna, J. P., Sun, S., and Siegfried, R. W., 2003. Instantaneous spectral analysis: Detection of low-frequency shadows associated with hydrocarbons. The Leading Edge, 22(2), 120-127.

Chapman, M., Liu, E., and Li X., 2005. The influence of abnormally high reservoir attenuation on the AVO signature. The Leading Edge, 24(11), 1120-1125.

Chen, X., He, Z., Huang, D., and Wen, X., 2009. Low frequency shadow detection of gas reservoirs in time-frequency domain. Chinese Journal of Geophysics, 52(1), 215-221.

Ebrom, D., 2004. The low-frequency gas shadow on seismic sections. The Leading Edge, 23(8), 772.

Goloshubin, G. M., and Korneev, V. A., 2000. Seismic low-frequency effects from fluid-saturated reservoir. SEG Technical Program Expanded Abstracts, 19, 1671-1674.

Goloshubin, G. M., Korneev, V. A., and Vingalov, V. M., 2002. Seismic low-frequency effects from oil-saturated reservoir zones. SEG Technical Program Expanded Abstracts, 21, 1813-1816.

Goloshubin, G. M., Silin, D. B., Vingalov, V., Takkand, G., and Latfullin, M., 2008. Reservoir permeability from seismic attribute analysis. The Leading Edge, 27(3), 376-381.

Korneev, V. A., Goloshubin, G. M., Daley, T. M., and Silin, D. B., 2004. Seismic low frequency effects in monitoring fluid-saturated reservoirs. Geophysics, 69(2), 522-532.

Liu, Y., 2004. Seismic “low frequency shadows” for gas sand reflection. SEG Technical Program Expanded Abstracts, 23, 1563-1566.

Liu, J., and Marfurt, K. J., 2007. Instantaneous spectral attributes to detect channel. Geophysics, 72(2), P23-P31.

Odebeatu, E., Zhang, J., and Chapman, M., 2006. Application of spectral decomposition to detection of dispersion anomalies associated with gas saturation. The Leading Edge, 25(2), 206-210.

Silin, D. B., Korneev, V. M., Goloshubin, G. M., and Patzek, T. W., 2004. A Hydrologic View on Biot’s Theory of Poroelasticity. LBNL Report 54459.

Tai, S., Puryear, C., and Castagna, J. P., 2009. Local frequency as a direct hydrocarbon indicator. SEG Technical Program Expanded Abstracts, 28, 2160-2164.

Taner, M. T., Koehler, F., Sheriff, R. E., 1979. Complex seismic trace analysis. Geophysics, 44(6), 1041-1063.

Wang, Y., 2007. Seismic time-frequency spectral decomposition by matching pursuit. Geophysics, 72(1), V13-P20.

Zeng, H., and Backus M. M., 2005. Optimizing thin-bed interpretation with 90°-phase wavelets. SEG Technical Program Expanded Abstracts, 24, 790-794